A Methodology for Evaluating Mixed-mode (I + II) SIF, Combining Experimental Data Acquired by ESPI with Westergaard Type Solution

Hadadian A[1,*], Afaghi Khatibi A[2] , Nikkhah M.[3] and Mohammadi F[4]

***Abstract*— In this study a symmetrical double exposure of He-Ne laser in an optical setup with the angle of 45o is used to determine stress intensity factors. Plexy glass specimens are subjected to external loads by a rotational single-axis loading system, and Electronic Speckle Pattern Interferometry (ESPI) approach is then used to determine the in-plane displacement around the crack-tip in inclined edge cracks under mix-mode loading. Processing displacement fringes with suitable filtering methods, stress intensity factors are then calculated using analytical solutions from linear elastic fracture mechanics (LEFM). The obtained results are then compared to those from finite element analysis and the other published results in the literature.**

***Index Terms*— Stress intensity factors, fracture mechanics, mix-mode loading, electronic speckle pattern interferometry (ESPI).**

I. Introduction

The concept of Linear Elastic Fracture Mechanics (LEFM) is widely used to determine the influence of cracks on structural integrity and their performance. Critical crack length calculation and equations for stress intensity factors in LEFM can be found in fracture mechanics handbooks [1]. In this type of publications, mostly only solutions for a specific mode of fracture have been addressed. This is despite of the fact that most practical problems are in mixed mode loading condition and therefore, assuming a single mode of fracture will lead to over simplification of these problems.

Variety of experimental methods has been utilized to evaluate stress intensity factors under different loading conditions. Among them reflected as well as transmitted caustics [2, 3], holographic interferometry [4] and Digital Speckle Pattern Interferometry system [5] can be mentioned. Although Humbert et al have used a Michelson interferometer to investigate out-of-plane displacement near the crack tip in plexy glass specimens, but evaluation of displacement field for mixed mode loading has not been reported [6]. Some researchers have attempted to improve ESPI approach by using more sensitive optical setups and implementing more accurate image processing methods [7,8].

Another aspect of optical based experimental mechanics is applying more robust techniques of image processing. Different attempts have been done to enhance the applied algorithms by least-square calculation of three correction parameters [9] as well as pixel shift correlation and summing up load steps [10]. H.J.Li et al have utilized a new point of view in using of wavelet transform maps of fringe patterns by statistics of phase modulations related to the object deformation [11]. Some authors reported that using spatial phase shifting can enhance the sensitivity [12]. Bhaduri et al have provided a complete comparison among different algorithms of phase-shifting in Digital speckle pattern interferometry (DSPI) [13].

Because of the plastic zone and high gradient of displacements and strains around the crack tip, experimental evaluation of the crack tip is not a simple task. In order to overcome this problem, Electronic Speckle Pattern Interferometry (ESPI) method with double exposure having high sensitivity to in-plane-displacement was utilized in this study. The displacement field was acquired experimentally and then by using LEFM equations, KI and KII stress intensity factors were determined.

II. THEORY OF ESPI

In Electronic Speckle Pattern Interferometry (ESPI) the fringe patterns introduce displacement contours. Due to the phase differences between deformed and un-deformed situations of any point on the specimen, these fringes can be captured.

To measure deformations in a perpendicular direction to the line of sight, i.e. the in-plane direction, a setup shown in Fig. 1 was used.

The laser beam is divided in two equal intensity beams which both illuminate the specimen. Both of illuminating beams reach the sample at equal angles of α. The image of unloaded specimen is captured by a CCD camera directed along the z-axis and in the plane of the collimated wave fronts. These wave fronts are scattered at the surface of sample and form a speckle pattern [14]. After applying the external loading, the second image which is the speckle pattern of the deformed sample is captured. These two

1 Department of Mechanical and Industrial Engineering, Concordia University, Montreal, Quebec, CANADA, (email: a_hadad@encs.concordia.ca)
2 Department of Mechanical Engineering, American University of Sharjah, P.O. Box 26666, Sharjah, UAE, (email: akhatibi@aus.edu)
3 Faculty of Mechanical Engineering, K. N. Toosi University of Technology, Tehran, Iran Faculty, (email: me.nikkhah@gmail.com)
4 Department of Mechanical and Industrial Engineering, Concordia University, Montreal, Quebec, CANADA, (email: far_moh@encs.concordia.ca)

ISBN: 978-988-18210-7-2
ISSN: 2078-0958 (Print); ISSN: 2078-0966 (Online)

speckle patterns are then processed using an appropriate image processing code. When the specimen is loaded, the test area undergoes a deformation and consequently a change in the speckle pattern is occurred.

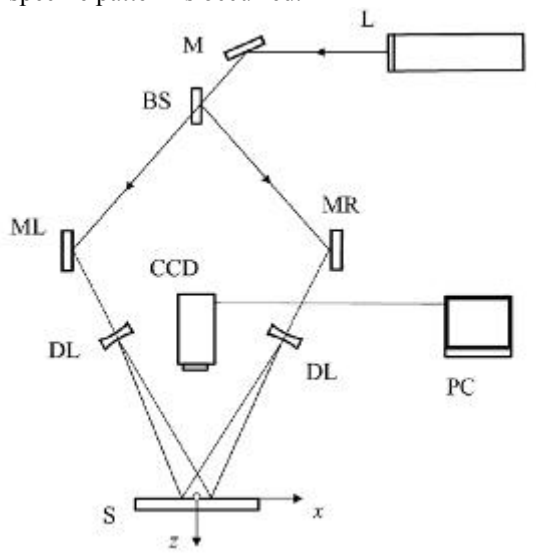

Fig1. ESPI system for measuring the in-plane displacement component u(x; y): L,10 mW He-Ne laser; BS,Beam-splitter; M, ML and MR, mirrors; DL, divergent lens; CCD, video camera; S, test specimen; PC, Digital image processing system.

The ESPI test software was used to process the two interference patterns corresponding to unloaded and loaded states of the specimen. The outcome of this process was alternate light and dark fringes. These fringes represent contours of equal displacement in the direction of x-axis. From ESPI theory, fringe spacing is given by [14]

$$\Delta x = \frac{d}{n} = \frac{\lambda d}{2\ \Delta d\ \sin\alpha} \tag{1}$$

From which the displacement Δd is obtained

$$\Delta d = \frac{n\lambda}{2\ \sin\alpha} \tag{2}$$

where λ is the wavelength of laser light, d is the measured reference length on the surface along the x-axis, Δd is the displacement of reference length in the direction of the x-axis, n is the number of fringes and α is the angle of inclination of coherent wave front to surface normal in z-plane. Any occurred distortion or having uneven size in fringes reveals structural abnormality or a defect.

After image processing and subtracting the images corresponding to loaded and unloaded cases, unwrapping processing of the fringes patterns can be implemented. Phase difference and displacements are related to each other by:

$$\Delta\phi = \frac{4\pi}{\lambda} u(x)\ \sin\alpha \tag{3}$$

where, λ is the wavelength of used laser source. It should be noted that the main shortcoming of this method is its high sensitivity to vibration and noises, as discussed in [14].

III. EXPERIMENT

A. Materials and geometry of specimens

In this work, PMMA specimens with E=2610 MPa and ν=0.34 were tested. They were Plexy glass plates with 3 mm thickness. For preparing notches, arbor milling cutter with 0.2 mm thickness in 1800 rpm was used. According to ASTM D638, whenever the length to width ratio is bigger than 4, it can be assumed that the stress in the middle of the specimen is uniform. Schematic of geometry with parameters and dimensions of test samples are shown in Fig.2 and Table 1 respectively.

After machining notches and for improving the quality of images as well as to prevent the light transmission through the specimens, all test samples were painted with a bright white color.

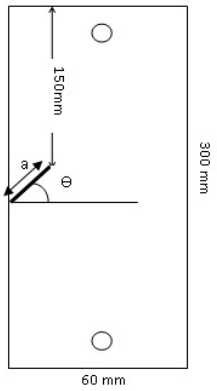

Fig2. Schematic view of specimens

Table 1: Dimensions of specimens

No.	length (mm)	width (mm)	thickness (mm)	Crack length(mm) a	Crack angle Θ
One	300	60	3	6	30
Two	300	60	3	12	30
Three	300	60	3	6	45
Four	300	60	3	12	45

B. Fracture mechanics equations

For mode I, mode II and mixed-mode cracks in plane stress problems, Westergaard type solution gives the displacement fields around the crack tip as [15]:

$$u_x = \sum_{n=1}^{\infty} \frac{A_{In}}{2G} r^{n/2} \left\{ m\ \cos\frac{n}{2}\theta - \frac{n}{2}\cos(\frac{n}{2}-2)\theta + \left(\frac{n}{2}+(-1)^n\right)\cos\frac{n}{2}\theta \right\} \tag{4}$$
$$- \sum_{n=1}^{\infty} \frac{A_{IIn}}{2G} r^{n/2} \left\{ m\ \sin\frac{n}{2}\theta - \frac{n}{2}\sin(\frac{n}{2}-2)\theta + \left(\frac{n}{2}+(-1)^n\right)\sin\frac{n}{2}\theta \right\}$$

$$u_y = \sum_{n=1}^{\infty} \frac{A_{In}}{2G} r^{n/2} \left\{ m\ \sin\frac{n}{2}\theta - \frac{n}{2}\sin(\frac{n}{2}-2)\theta - \left(\frac{n}{2}+(-1)^n\right)\sin\frac{n}{2}\theta \right\} \tag{5}$$
$$- \sum_{n=1}^{\infty} \frac{A_{IIn}}{2G} r^{n/2} \left\{ -m\ \cos\frac{n}{2}\theta - \frac{n}{2}\cos(\frac{n}{2}-2)\theta + \left(\frac{n}{2}-(-1)^n\right)\cos\frac{n}{2}\theta \right\}$$

Where u_x and u_y are displacement components, G is the shear modulus; m is for plane stress and for plane strain, is the Poisson ratio and r and θ, respectively, express the polar coordinate around the crack tip as shown in Fig. 3.

ISBN: 978-988-18210-7-2
ISSN: 2078-0958 (Print); ISSN: 2078-0966 (Online)

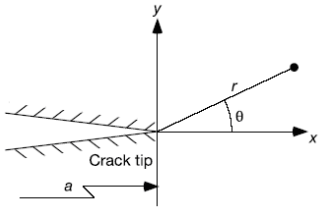

Fig.3. Polar coordinate around the crack tip

In series solution, the coefficient of first terms AI1 and AI2 relate to KI and KII stress intensity factors through the following equation.

$$A_{I1} = \frac{K_I}{\sqrt{2\pi}} \quad \text{and} \quad A_{II1} = -\frac{K_{II}}{\sqrt{2\pi}} \tag{6}$$

Shchepinov et al. [16] showed that considering only the first term for stress intensity factor determination at small distances from the crack tip will need a correction coefficient equal to 0.998. Also from the algebraic point of view it can be noted that when R closes to zero, it is possible to eliminate the higher order terms. By considering only the first terms, equations (4) and (5) can be rewritten as:

$$u_x = \frac{K_I}{4G\sqrt{2\pi}} r^{1/2}\left\{(2m-1)\ \cos\frac{\theta}{2} - \cos\frac{3\theta}{2}\right\} - \frac{K_{II}}{4G\sqrt{2\pi}} r^{1/2}\left\{(m-3)\ \sin\frac{\theta}{2} + \sin\frac{3\theta}{2}\right\} \tag{7}$$

$$u_y = \frac{K_I}{4G\sqrt{2\pi}} r^{1/2}\left\{(2m+1)\ \sin\frac{\theta}{2} - \sin\frac{3\theta}{2}\right\} - \frac{K_{II}}{4G\sqrt{2\pi}} r^{1/2}\left\{(3-2m)\ \cos\frac{\theta}{2} - \cos\frac{3\theta}{2}\right\} \tag{8}$$

But as mentioned before, the measurement system can measure the displacement in X and Y directions. From coordinate transformation law, we can restate the displacements as

$$u_x = u_X \cos\beta + u_Y \sin\beta$$
$$u_y = -u_X \sin\beta + u_Y \cos\beta \tag{9}$$

where, β is the crack angle.

C. Procedure of experiment

The experimental setup is shown in Fig.4. This setup has only one sensitive vector in the x-direction .Consequently for measuring the y component of displacement, specimens must be rotated 90o to adjust its y-axis to sensitive vector of optical setup (x-direction).

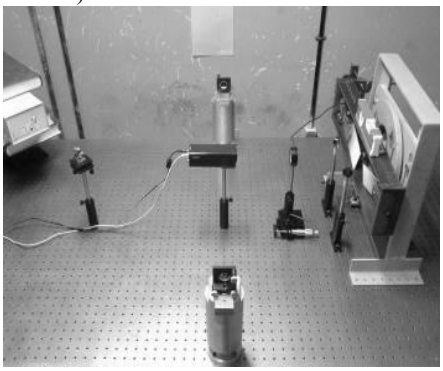

Fig.4: Optical setup used in this study

Rotational single axis loading machine was designed and manufactured for this purpose. A photo of the loading machine is displayed in Fig5. It is adjustable in both x and y directions in order to align the study area of the specimen to the detectable zone of optical setup.

Fig .5: Rotational single axis loading machine at 45°

The following steps are done in the experiment:

1- The loading machine is set in such a way that the desired area becomes the center of rotation.

2- Unloading condition images (speckle patterns) are captured in both x and y direction as bench-mark images (Fig. 6a, b).

3- The specimen is then loaded.

4- In x direction the speckle pattern is captured and saved. Then, the loading machine is rotated and y image (speckle pattern) of the specimen at that load is captured in the same way (Fig. 7a, b).

(a)

(b)

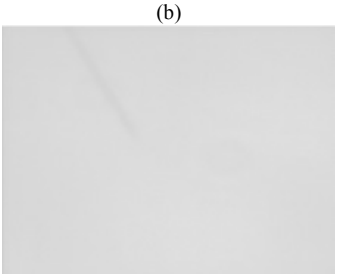

Fig. 6: Captured speckle patterns in unloading condition in specimen number 2 (a) in x-direction, (b) in y-direction

(a)

(b)

ISBN: 978-988-18210-7-2
ISSN: 2078-0958 (Print); ISSN: 2078-0966 (Online)

Fig. 7: Captured speckle patterns under 49 N in specimen number 2, (a) in x-direction, (b) in y-direction

5- The saved images are processed using a home-developed MATLAB© toolbox that utilizes the functions of XteremeFringeLib© software. In this step, each control image is subtracted from the corresponding loading image.

6- Image processing is accomplished on the images; consequently, fringe patterns and unwrapped phases are achieved respectively. Figs 8-11.

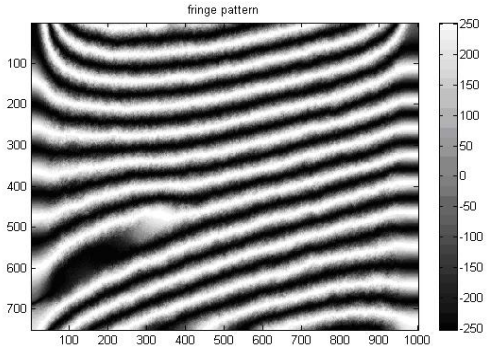

Fig.8: Displacement fringe patterns in X-direction for specimen number 2 under 49 N. The crack and its tip are indicated.

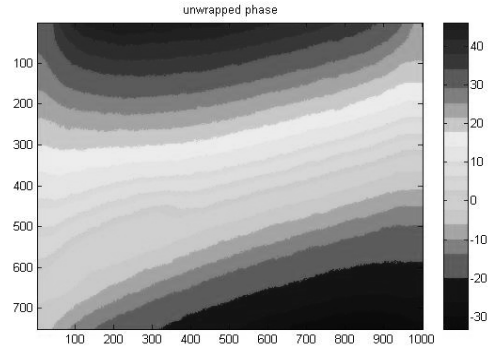

Fig.9: Unwrapped phase in X-direction for specimen number 2 under 49 N

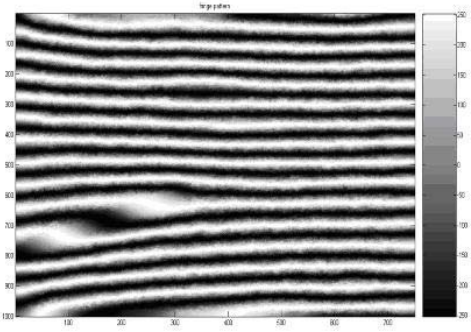

Fig.10: Displacement fringe patterns in Y-direction for specimen number 2 under 49 N

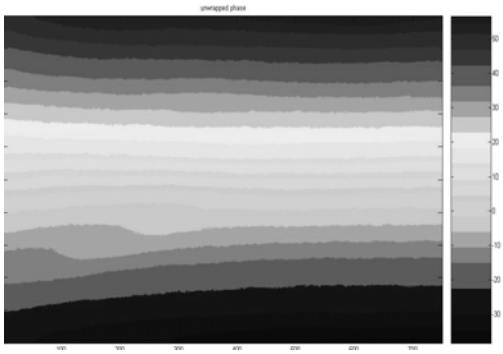

Fig.11: Unwrapped phase in Y-direction for specimen number 2 under 49 N

D. Calculations

In each unwrapped phase map and in the area of a ring with inner and outer radius of 1 mm and 2 mm, respectively, ten points are selected. This region is chosen because the distance between each selected point and the crack tip must long enough to avoid entering to the plastic zone around the crack tip; and, on the other hand, this distance should be small enough to satisfy the condition of LEFM theories. Therefore, instead of gathering data on only one distinct fringe; as it is done by other researches [16], data from ten arbitrary points in the above mentioned region were collected. These points are belonging to different contours of displacement which are visible as fringe patterns in wrapped maps. From these phases and collected data, displacement components of uX and uY are calculated by substituting appropriate values in equation (3). Then, by using resulted uX and uY in equation (9) as well as values for r and θ, the displacement equations of each point in local coordinate system are found. It is necessary to have the results in this type of coordinate system since fracture equations (7) and (8) are also expressed in a similar system. As a result, by using 10 points, 20 linear algebraic equations with 2 unknown parameters, namely KI and KII will be formed. Solving over-defined system of equations by least square method, the best solution of equations as stress intensity factors is achieved.

IV. Results

Four specimens were loaded in every 9.8 N increments. For each steps stress intensity factors were calculated and compared with results of other approaches. In this paper, only displacement fringe patterns and unwrapped phase maps in x and y-directions for specimen No.2 are shown in Fig. 9-11. Because of the unavailability of piezo-mounted mirrors in our laboratory, software techniques were used for phase extraction.

From each unwrapped phase map of specimens under the applied load and using arbitrary points around the crack tip, the values of φ_X and φ_Y are read. Then using Eq. (3), displacement components of u_X, u_Y are calculated. By substituting these values in equations (9) and then (7), (8), the values of u_x and u_Y are determined. Evaluated stress intensity factors from this study as well as those calculated using FEM and Theocaris's equations [3] are shown Fig.12-15.

ISBN: 978-988-18210-7-2
ISSN: 2078-0958 (Print); ISSN: 2078-0966 (Online)

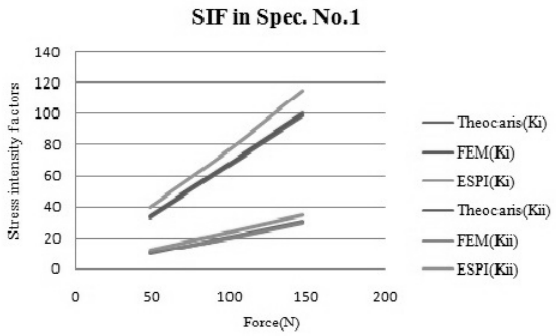

Fig.12: Stress intensity factors in Specimen No.1

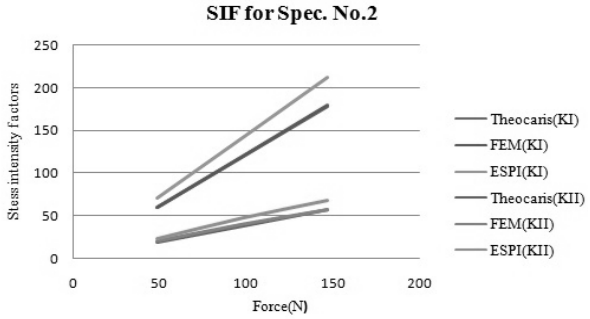

Fig.13: Stress intensity factors in Specimen No.2

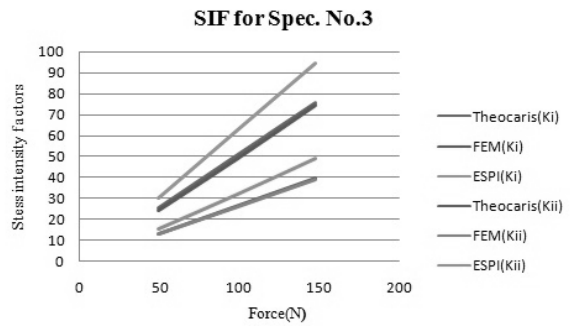

Fig. 14: Stress intensity factors in Specimen No.3

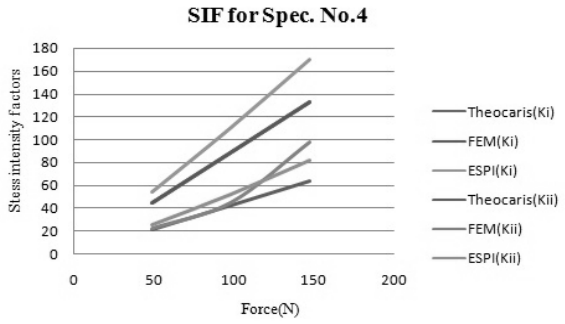

Fig.15: Stress intensity factors in Specimen No.4

Figures clearly reveal that in all cases FEM results are in good agreements with the Theocaris's results exempt for KII of specimen No.4 because it has longer crack length with larger crack angle. This can easily lead to significant contribution of the second mode. In addition, greater stress around the crack tip can have significant effects on the assumptions of LEFM in FEM modeling which is observed as less agreement with the experimental results. However, the results behave in the same way in both experimental approaches.

According to the plots, in all cases ESPI overestimates the stress intensity factors. The overestimation of the SIF can have different reasons. But the most important factor in this current work is rigid body displacements. Since implemented image processing algorithms cancel the rigid motion approximately equal to 3.4 μm, so the implied rigid body motions have been affected in the measured displacements and consequently that will be the case for the evaluated stress intensity factors. As result, developing a better program that can cancel the occurred rigid body displacements can improve results and decrease errors effectively.

V. CONCLUSION

In this research, ESPI method with Westergaard type solution was implemented to evaluate KI and KII stress intensity factors in inclined edge cracks of isotropic materials under mixed-mode loading. For this purpose, phase differences for each selected point in X and Y paired images was used to calculate uX and uY. Then by using the transformation law ux and uy were calculated. By utilizing LEFM formulas, an over-defined system of equations was derived for the stress intensity factors. In comparison with other methods, evaluated stress intensity factors from this study show maximum difference of 19.2%, which in general qualifies the using of ESPI method as a low cost approach for mixed-load conditions in experimental fracture mechanics.

REFERENCES

[1] Broek D ,The practical use of fracture mechanics, KLUWER ACADEMIC PUBLISHER, The Netherlands, 1988.

[2] Theocaris P.S., Gdoutos E. An optical method for determining opening mode and edge sliding mode stress intensity factors. *J Appl Mech*., 1972, Vol.**7**, pp.91-97.

[3] Theocaris P.S., Papadopoulos G.A. The influence of edge-cracked plates on K_I and K_{II} component of stress intensity factors, studied by caustics. *J.Phys. D:Appl*, 1984, Vol.**17**, pp. 2339-2349.

[4] Macha D.E. , Sharpe W.N. , Grandte A.F. A laser interferometry method for experimental stress intensity factor calibration. *Cracks and Fracture*, ASTM-STP, Vol. **601**, American Society for Testing and Materials, Philadelphia, 1976, pp. 490-500.

[5] Diaz F.V., Kaufmann G.H., Armas A.F., Möller O. , Measurement of near-tip displacement field in a fatigue damage steel plate by digital speckle pattern interferometry. *Opt Laser Eng*, 2002,Vol. **37**, pp. 621-629.

[6] Humbert L, Valle V , Cottron M , Experimental determination and empirical representation of out-of-plane displacements in a crack elastic plate loaded in mode I. Int J Solids and Struct, 2000, Vol. **37**, pp. 5493-5504.

[7] Gundu P.N, Hack E, Rastogi P. Adaptive optics interferometer using superspeckles for high resolution deformation measurement. *Opt Commun*, 2007, Vol. **278**, pp. 382-386

[8] Martínez A, Rayas J.A , Cordero R, Genovese K. Analysis of optical configurations for ESPI. *Opt Laser Eng* , 2008, Vol. **46**, pp. 48-54.

[9] Dolinkoa A.E, Kaufmann G.H , A least-squares method to cancel rigid body displacements in a hole drilling and DSPI system for measuring residual stresses. *Opt Laser Eng* ,2006, Vol. **44**, pp. 1336-1347.

[10] Hack E , and Schumacherb A, DSPI strain measurement on an externally reinforced bending beam: A comparison of step-by-step addition and pixel shift correlation. Opt Laser Eng, 2007, Vol.**45**, pp.589-595.

[11] Li H.J, Chen H.J, Zhang J, Xiong C.Y, Fang J. Statistical searching of deformation phases on wavelet transform maps of fringe patterns. *Opt Laser Technol*, 2007, Vol. **39**, pp. 275-281.

[12] Bhaduri B, Kothiyal M.P, Mohan N.K , Digital speckle pattern interferometry (DSPI) with increased sensitivity: Use of spatial phase shifting. *Opt Commun*, 2007, Vol. **272**, pp. 9-14.

ISBN: 978-988-18210-7-2
ISSN: 2078-0958 (Print); ISSN: 2078-0966 (Online)

[13] Bhaduri B, Kothiyal M.P and Mohan N.K, Comparative study of phase-shifting algorithms in digital speckle pattern interferometry. *Optik - Int J Light Electron Opt*, 2008,Vol.**119**, pp. 147-152.
[14] Rastogi PK, editor. Digital speckle pattern interferometery and related techniques. 2001, Willey.
[15] Broek D , Elementary Engineering Fracture Mechanics. Martinus Nijhoff Publishers, 1984, The Netherlands.
[16] Shchepinov, V.P., Pisarev, V.P., strain and stress analysis by Holography and Speckle Interferometry, 1996, Wiley.

ISBN: 978-988-18210-7-2
ISSN: 2078-0958 (Print); ISSN: 2078-0966 (Online)